Mem. S.A.It. Vol. 85, 548

Memorie della

Primordial enrichment of the first galaxies

John H. Wise[1], Matthew J. Turk[2], Michael L. Norman[3], Tom Abel[4]

[1] Center for Relativistic Astrophysics, School of Physics, Georgia Institute of Technology, 837 State Street, Atlanta, GA 30332, USA, e-mail: jwise@gatech.edu
[2] Department of Astronomy, Columbia University, 538 West 120th Street, New York, NY 10027, USA
[3] Center for Astrophysics and Space Sciences, University of California at San Diego, La Jolla, CA 92093, USA
[4] Kavli Institute for Particle Astrophysics and Cosmology, Stanford University, Menlo Park, CA 94025, USA

Abstract. We present an adaptive mesh refinement radiation hydrodynamics simulation that follows the transition from Population III to Population II star formation. A top-heavy initial mass function for the Population III stars is considered, resulting in a plausible distribution of pair-instability supernovae and associated metal enrichment. We find that the gas fraction recovers from 5 percent to nearly the cosmic fraction in halos with merger histories rich in halos above $10^7 M_\odot$. A single pair-instability supernova is sufficient to enrich the host halo to a metallicity floor of $10^{-3} Z_\odot$ and to transition to Population II star formation. We find that stellar metallicities do not necessarily trace stellar ages, as mergers of halos with established stellar populations can create superpositions of $t - Z$ evolutionary tracks.

Key words. cosmology — methods: numerical — hydrodynamics — radiative transfer — star formation

1. Introduction

The first (Pop III) stars are metal-free and have some large characteristic mass. Recent work has suggested that fragmentation may occur on scales of 1000–2000 AU prior to the formation of the first protostar, resulting in high-mass, low-multiplicity groups (Turk et al., 2009; Stacy et al., 2010; Greif et al., 2011). A fraction of these high-mass, metal-free stars enriches the surrounding intergalactic medium (IGM) when they go supernova (SN), which occur in stars with $\lesssim 40 M_\odot$ in Type II supernovae (SNe) or in stars roughly between 140 $M_\odot$ and 260 $M_\odot$ in pair-instability SNe (PISNe; Heger & Woosley, 2002). The host halo and the neighboring halos are then enriched with this ejecta. There exists a critical metallicity that is between $10^{-6}\,Z_\odot$ and $10^{-4}\,Z_\odot$, depending on how strong dust cooling in these environments.

Pop III stars primarily form in dark matter (DM) halos with $M \sim 10^6 M_\odot$. Their stellar radiation ionizes and heats an H II region with a radius 1–3 kpc. The overpressurized H II region drives a 30 km s^{-1} shock that is 10 times greater than the escape velocity of the halo, leaving behind a warm (3×10^4 K) and diffuse (0.5cm^{-3}) medium (Kitayama et al., 2004; Whalen et al., 2004; Abel et al., 2007). The transition from Pop III to Pop II star formation (SF) is solely dependent on the propagation of metals from the SNe remnants into future sites of SF. Their flows are complex because of the interactions between the SN blast wave, cosmological accretion, halo mergers, and nearby stellar feedback. Numerical simulations are useful to detangle and study these complexities and the transition from Pop III to Pop II stars. Here, we present a simulation that includes both types of SF, and their radiative and mechanical feedback. The methods used here incorporate and link together recent results from metal-enriched and metal-free star formation, the critical metallicity, and pair-instability supernovae.

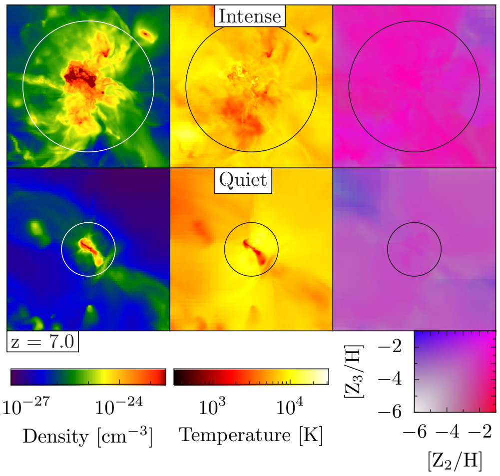

Fig. 1. Density-weighted projections of density (left), temperature (center), and metallicity (right) of the two selected halos at $z = 7$. The field of view is 5 proper kpc, and the circles have a radius of r_{200}. The metallicity projections are a composite image of metals originating from Pop II (red) and III (blue) stars with magenta indicating a mixture of the two. From Wise et al. (2012) reproduced with the permission of AAS.

2. Simulation setup

We use the adaptive mesh refinement (AMR) code ENZO v2.0[1] (The Enzo Collaboration et al., 2013). We use the nine-species (H I, H II, He I, He II, He III, e^-, H_2, H_2^+, H^-) non-equilibrium chemistry model in ENZO (Abel et al., 1997; Anninos et al., 1997; Glover & Abel, 2008). We spatially distinguish metal enrichment from Pop II and Pop III stars.

To resolve minihalos with at least 100 dark matter (DM) particles and follow the formation of the first generation of dwarf galaxies, we use a simulation box of 1 Mpc that has a resolution of 256^3. This gives us a DM mass resolution of 1840 $M_\odot$. We refine the grid on baryon overdensities of $3 \times 2^{-0.2l}$, where l is the AMR level, resulting in a super-Lagrangian behavior. We also refine on a DM overdensity of three and always resolve the local Jeans length by at least 4 cells, avoiding artificial fragmentation during gaseous collapses (Truelove et al., 1997). If any of these criteria are met in a single cell, it is flagged for further spatial refinement.

We initialize the simulation with GRAFIC (Bertschinger, 2001) at $z = 130$ and use the cosmological parameters from the 7-year WMAP ΛCDM+SZ+LENS best fit (Komatsu et al., 2011): $\Omega_M = 0.266$, $\Omega_\Lambda = 0.734$, $\Omega_b = 0.0449$, $h = 0.71$, $\sigma_8 = 0.81$, and $n = 0.963$ with the variables having their usual definitions. We use a maximum refinement level of $l = 12$, resulting in a maximal comoving resolution of 1 pc.

We distinguish Pop II and Pop III SF by the total metallicity of the densest cell in the molecular cloud. Pop II stars are formed if [Z/H] > −4, and Pop III stars are formed otherwise. For more details and justifications, we refer the reader to Wise et al. (2012). We model individual Pop III stars with mass-dependent luminosities, lifetimes, and stellar endpoints Schaerer (2002); Heger et al. (2003). The Pop II model treats stellar clusters with a Salpeter IMF as single star particles with a minimum mass of 1000 $M_\odot$. Stellar radiation is transported using ENZO+MORAY (Wise & Abel, 2011) from all Pop III stars and young (< 20 Myr) Pop II stellar clusters. All of the analysis and plots were made with `yt` (Turk et al., 2011).

3. Results

Here we present the gaseous and stellar evolution of two selected halos in the simulation: one that has an early mass buildup but no ma-

[1] enzo-project.org, changeset b86d8ba026d6

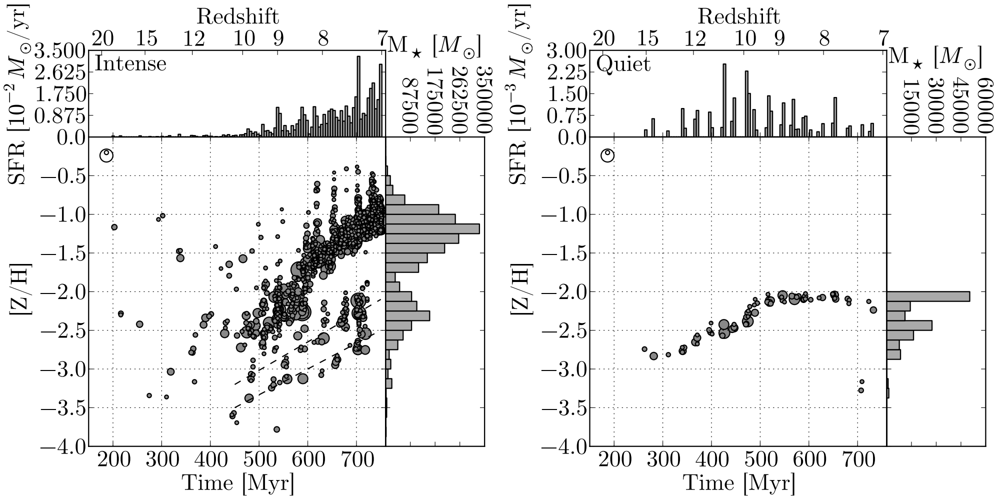

Fig. 2. The scatter plots show the metal-enriched (Pop II) star formation history of the intense (top) and quiet (bottom) halos as a function of total metallicity, i.e. the sum of metal ejecta from both Pop II and Pop III SNe, at $z = 7$. Each circle represents a star cluster, whose area is proportional to its mass. The open circles in the upper right represent 10^3 and 10^4 $M_\odot$ star clusters. The upper histogram shows the SFR. The right histogram depicts the stellar metallicity distribution. From Wise et al. (2012) reproduced with the permission of AAS.

jor mergers after $z = 12$, and one that experiences a series of major mergers between $z = 10$ and $z = 7$. We name the halos "quiet" and "intense", respectively. The entire simulation contains 38 galaxies with 3640 Pop II stellar clusters and captures the formation of 333 Pop III stars. We illustrate the state of these two galaxies at $z = 7$ in Figure 1 with density weighted projections of gas density, temperature, and metallicity. Radiative and mechanical feedback create a multi-phase medium inside these halos, which are embedded in a warm and ionized IGM.

Figure 2 shows the SF history (SFH), metallicity distribution, and SF rates (SFR) of both halos. A nearby PISNe provides a metallicity floor of [Z/H] = –2.8 in the quiet halo at which metallicity the first Pop II stars form. The stellar metallicity evolution exhibits what is expected from an isolated system with the stellar feedback steadily enriching the ISM, resulting in a correlation between stellar age and metallicity. After $z = 10$ the metallicities plateau at [Z/H] = –2.1 for reasons previously discussed. The SFR peaks at $z = 10$ and decreases as the cold gas reservoir is depleted. Around $z = 7.5$, a 25:1 minor merger occurs, and the gas inside the satellite halo is compressed, triggering metal-poor, [Z/H] = –3.2, SF during its nearest approach. This halo remains metal-poor because most of metal enrichment in the quiet halo occurs in bi-polar flows perpendicular to the galaxy disk and filament. Stars with [Z/H] < –3 compose 1.6 percent of the total stellar mass.

In contrast with the quiet halo, the intense halo undergoes a few mergers of halos with an established stellar population. This creates a superposition of age-metallicity tracks in the SFH, seen in the complexity of Figure 2. The first two Pop II stellar clusters have an unexpectedly high metallicity [Z/H] ~ –1, which occurs when a PISN blastwave triggers SF in two neighboring halos. Most of the early SF have [Z/H] = –2.5. At $z = 9$, the halo's virial temperature reaches 10^4 K. This combined with a 10:1 merger creates a starburst that quickly enriches the halo to [Z/H] = –1.5 by $z = 8$. The halo continues to enrich itself afterwards. The spikes in the scatter plot corre-

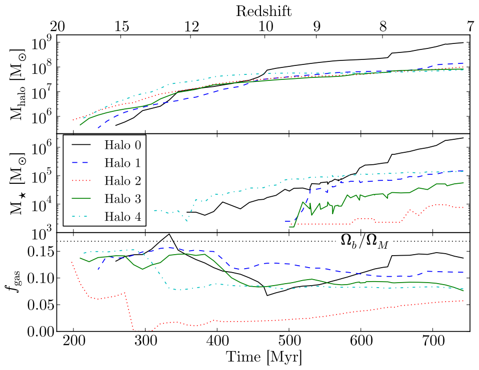

Fig. 3. Evolution of the total halo mass (top), stellar mass (middle), and gas fraction (bottom) of the five most massive halos at z = 7, where the intense and quiet halos are Halo 0 and 4, respectively. From Wise et al. (2012) reproduced with the permission of AAS.

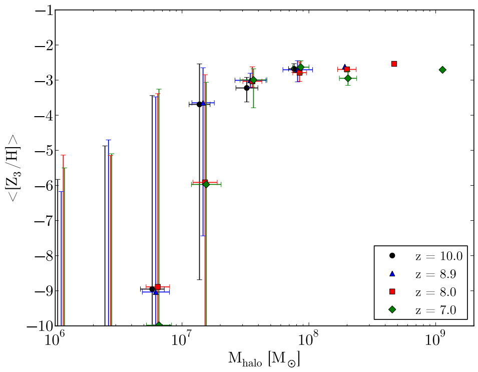

Fig. 4. Average halo metallicity from Pop III SNe as a function of total halo mass. Inhomogeneous metal enrichment causes the large spread in metallicity at low masses. At $M_{halo} > 3 \times 10^7 M_\odot$, all halos are enriched by Pop III SNe above [Z/H] > -4. From Wise et al. (2012) reproduced with the permission of AAS.

spond to SN triggered SF in nearby molecular clouds that are enriched up to a factor of 10 with respect to the ISM. However their mass fraction are small compared to the total stellar mass. The starburst at z = 9 creates a bimodal metallicity distribution with peaks at [Z/H] = –2.4 and –1.2 with the metal-rich component mainly being created after the starburst. Two systems with sizable stellar components merge into the halo at $z \sim 8$, and their stellar populations, which are traced by dashed lines in Figure 2, are still discernible in the metallicity-age plot. Stars with [Z/H] < –3 compose 1.8 percent of the total stellar mass.

To further demonstrate the metallicity floor in high-redshift dwarf galaxies, we show the average metallicity from Pop III SNe [Z_3/H] in all halos as a function of halo mass at z = 7, 8, 9, and 10 in Fig. 4, and it is strongly dependent on halo mass. The [Z_3/H] error bars mark the 25% and 75% percentiles of the distribution at $M = M_{halo}$ because the underlying distribution is not necessarily Gaussian at all halo masses. Above $3 \times 10^7 M_\odot$, all halos enriched to [Z_3/H] $\gtrsim -4$ with little time evolution, further illustrating the metallicity floor. Below this halo mass, the distribution is roughly bimodal composed of pristine and metal-enriched halos.

Figure 3 shows the total, metal-enriched stellar, and gas mass history of the most massive progenitors of the five most massive halos. The quiet halo (halo 4) undergoes a series of major mergers at $z > 12$, growing by a factor of 30 to $2.5 \times 10^7 M_\odot$ within 150 Myr. Afterwards it only grows by a factor of 3 by z = 7 mainly through smooth accretion from the filaments and IGM. At the same time, the intense halo (halo 0) has a mass $M = 3 \times 10^6 M_\odot$, but it is contained in a biased region. After z = 10, halos in this region merge to form a $10^9 M_\odot$ halo at z = 7 with two major mergers at redshifts 10 and 7.9, seen in the rapid increases in total mass. The merger history of the two halos are not atypical as dark matter halos can experience both quiescent and vigorous mass accretion rates. Furthermore, there can be a considerable spread in stellar mass fraction, as seen in halos 1–4 having $M \simeq 10^8 M_\odot$ with their stellar masses ranging from $10^3 M_\odot$ to $2 \times 10^5 M_\odot$. This spread in the $M_\star - M_{vir}$ relation is most directly linked to the differing gas fraction histories, seen in the bottom panel of Figure 3. The changes in gas fraction are mainly caused by the (Pop III) star formation histories and environment.

The gas fractions of both halos decrease from 0.15 to 0.08 by outflows driven by ionization fronts and blastwaves in their initial starbursts. The quiet halo does not have a merger with a gas-rich halo. These infalling low-mass halos are photo-evaporated, hosting diffuse warm gas reservoirs instead of cold dense cores. After $z = 10$, the halo mainly accretes warm diffuse gas from the filaments and IGM. In contrast, the intense halo grows from major mergers of halos with gas-rich halos. The progenitor halos involved in the major mergers are able to host molecular clouds and have higher gas fractions. Between $z = 10$ and $z = 8$, the gas fraction increases from 0.07 to 0.12 until it jumps to 0.14 when a gas-rich major merger occurs. The stellar mass accordingly increases with the ample supply of gas during this period.

4. Summary

We focus on the birth of two galaxies prior to reionization with a cosmological AMR radiation hydrodynamics simulation. Supernovae from Pop III stars provide the necessary heavy elements for the transition to a Pop II stellar population, which we have directly simulated. We find that one PISN is sufficient to enrich the star-forming halo and surrounding $\sim$ 5 kpc to a metallicity of $10^{-3} Z_\odot$, given $M_{\rm char} = 100\ M_\odot$. DLA systems have a metallicity floor on the same order (Wolfe et al., 2005; Penprase et al., 2010), and metal enrichment from Pop III SNe provides a possible explanation (Kobayashi et al., 2011). Our simulation strengthens this claim of a metallicity floor from Pop III SNe (e.g. Tornatore et al., 2007; Maio et al., 2011), where our work improves on previous studies by resolving star-forming molecular clouds and employing more realistic feedback physics, in particular, radiation transport. To conclude, we have shown that it is possible to simulate the formation of a high-redshift dwarf galaxy and its entire SFH with radiative and mechanical feedback. These results provide invaluable insight on the first galaxies and the role of metal-free stars in the early universe.

References

Abel, T., et al. 1997, New Astron., 2, 181

Abel, T., Wise, J. H., & Bryan, G. L. 2007, ApJ, 659, L87

Anninos, P., et al. 1997, New Astron., 2, 209

Bertschinger, E. 2001, ApJS, 137, 1

Glover, S. C. O., & Abel, T. 2008, MNRAS, 388, 1627

Greif, T. H., Springel, V., White, S. D. M. et al. 2011, ApJ, 737, 75

Heger, A., & Woosley, S. E. 2002, ApJ, 567, 532

Heger, A., et al. 2003, ApJ, 591, 288

Kitayama, T., et al. 2004, ApJ, 613, 631

Kobayashi, C., Tominaga, N., & Nomoto, K. 2011, ApJ, 730, L14

Komatsu, E., et al. 2011, ApJS, 192, 18

Maio, U., et al. 2011, MNRAS, 414, 1145

Penprase, B. E., et al. 2010, ApJ, 721, 1

Schaerer, D. 2002, A&A, 382, 28

Stacy, A., Greif, T. H., & Bromm, V. 2010, MNRAS, 403, 45

The Enzo Collaboration, et al. 2013, ArXiv e-prints (1307.2265)

Tornatore, L., Ferrara, A., & Schneider, R. 2007, MNRAS, 382, 945

Truelove, J. K., Klein, R. I., McKee, C. F. et al. 1997, ApJ, 489, L179

Turk, M. J., Abel, T., & O'Shea, B. 2009, Science, 325, 601

Turk, M. J., Smith, B. D., Oishi, J. S. et al. 2011, ApJS, 192, 9

Whalen, D., Abel, T., & Norman, M. L. 2004, ApJ, 610, 14

Wise, J. H., & Abel, T. 2011, MNRAS, 414, 3458

Wise, J. H., et al. 2012, ApJ, 745, 50

Wolfe, A. M., Gawiser, E., & Prochaska, J. X. 2005, ARA&A, 43, 861